MDPI

Article

Investigation of the Microstructure, Thermal Properties, and Mechanical Properties of Sn-Bi-Ag and Sn-Bi-Ag-Si Low Temperature Lead-Free Solder Alloys

Sheng Chen [1,†], Xinbao Wang [1,†], Zhiqiu Guo [2,*], Changjun Wu [1], Yongxiong Liu [3], Ya Liu [1,*] and Xuping Su [1]

1 Jiangsu Key Laboratory of Material Surface Science and Technology, Changzhou University, Changzhou 213164, China
2 Jinko Solar Co., Ltd., Haining 314416, China
3 School of Materials Science and Engineering, Xiangtan University, Xiangtan 411105, China
* Correspondence: zhiqiu.guo@jinkosolar.com (Z.G.); yliu@cczu.edu.cn (Y.L.)
† These authors contributed equally to this work.

Abstract: In this study, we investigated the microstructure, mechanical properties, and thermal performance of Sn-xBi-1Ag (x = 35, 37, 45, and 47 wt.%) solders, with a particular focus on the effect of adding trace Si atoms. The impact of different Ag concentrations on the properties of Sn-xBi-Ag-0.5Si solders was also studied. The results indicated that as the amount of Bi added to Sn-xBi-1Ag solder alloys increased, the tensile strength, microhardness, melting temperature, and melting range decreased somewhat, but the wettability improved. The Cu_6Sn_5 layer between the soldering alloy and the Cu substrate became thinner upon increasing the Bi content. Adding microcrystalline Si atoms to the Sn-Bi-1Ag alloy improved the tensile strength and microhardness, but the melting point and melting range were not significantly changed. The wettability was optimized, and the diffusion layer formed with the Cu matrix was significantly thinner. By increasing the Ag content in the Sn-Bi-(1,3)Ag-0.5Si alloy, the tensile strength of the alloy was continuously strengthened, while the hardness decreased slightly and the melting point and melting range increased slightly. The wettability was greatly improved, and the Cu_6Sn_5 layer became thinner.

1. Introduction

Sn-Pb alloys have been the primary solder alloys due to their excellent wettability, mechanical properties, and appropriate price [1–5]. However, Sn-Pb solders can no longer satisfy the demands of current industrial development due to increased environmental consciousness and the introduction of Restriction of Hazardous Substances (RoHS) and Waste Electrical and Electronic Equipment (WEEE) standards [6–8]. As a result, various types of lead-free solders, such as Sn-Zn and Sn-Ag, have been suggested as replacements [9–14]. Sn-Bi alloys are ideal lead-free solders because of their non-toxicity and lower melting point [15–17]. However, the inherent brittleness after adding Bi atoms results in poor solder reliability [18–20]. The wettability of Sn-Bi solder alloys is much lower than that of conventional Sn-40Pb solders, and the bias of Bi at the solder/Cu interface causes joint embrittlement, which greatly reduces the strength of the solder joint [21–25].

Because of its excellent conductivity and wettability, Ag is often added to Sn-Bi solders to enhance their properties [26–28]. Yang et al. [29] added Ag to a Sn-58Bi solder and found that the Ag_3Sn phase was formed in the alloy, which had fine-grain strengthening and second-phase strengthening effects that improved the solder's tensile strength. A modest quantity of Ag added to the Sn-58Bi solder also enhanced its microhardness [30]. Dong et al. [31] found that the addition of Ag accelerated the wetting reaction's speed and enhanced the Sn-58Bi solder's wettability. Wang et al. [32] further investigated the impact

of Ag on the wetting of a Sn-58Bi solder. As a result, the addition of Ag not only optimized the wettability but also restrained the development of the IMC layer (intermetallic layer) at the interface and enhanced the shear strength of the joint. Furthermore, low-eutectic Sn-Bi solders have better mechanical properties than eutectic Sn-Bi solders [33–36].

Currently, research on Sn-Bi-Ag solders has predominantly focused on the eutectic part (Sn-58Bi) and the hypoeutectic part (Sn-10Bi), but eutectic solders have weak mechanical properties, while hypoeutectic solders have a high melting point. There is little systematic data on Sn-xBi-Ag (x = 30–50) solders. In addition, during the hot-dipping of Zn-Al alloys, the addition of an appropriate amount of Si to the molten pool repressed the development of the intermetallic layer at the coating/steel interface [37,38]. However, there is limited information about the effect of Si on the properties of Sn-Bi-Ag solder alloys.

The purpose of this work was to study the microstructure, melting point, mechanical properties, wetting, and interface interactions of Sn-xBi-1Ag (x = 35, 37, 45, and 47 wt.%). The impact of the Si content on the characteristics of the Sn-Bi-Ag solder alloy and the IMC layer formed at the solder/Cu interface, as well as the effect of the Ag content on the properties of Sn-Bi-Ag-Si alloy solder, were also investigated.

2. Experimental Procedure

Sn particles, Bi blocks, Ag particles, and Si pieces with a purity of 99.99% were utilized in this experiment. Appropriate amounts of pure elements were weighed based on their nominal constituents. An aggregate mixture weighing 100 g for each solder was measured. The mixture was sealed in a vacuum quartz tube under an argon environment, melted at 300 °C for 12 h, and finally quenched in cold water. To promote reactions between components while heating, the quartz tube was shaken upside down for 2 min every 30 min during melting. To verify the sample's composition uniformity, the quenched sample was repeatedly melted three times according to the above heat treatment process.

For the Sn-Bi-Ag-Si solders, due to a huge difference between the melting points of Ag (961.3 °C), Si (1410 °C), Sn (231.89 °C), and Bi (271.5 °C), the Ag-0.5Si master alloy was initially synthesized by arc-melting in a high Ti-gettered argon atmosphere with a non-consumable tungsten electrode and a water-cooled Cu case. The prepared Ag-0.5Si master alloy sample was sealed in a vacuum quartz tube under an argon atmosphere, annealed at 1000 °C for 7 days, and finally water quenched. Then, an appropriate amount of Sn particles, Bi particles, and Ag-0.5Si alloy were sealed in a vacuum quartz tube under an argon atmosphere, melted at 480 °C for 12 h, and quenched in water. All samples were homogenized by melting three times. A schematic diagram of the samples' preparation is shown in Figure 1.

(a)

Figure 1. *Cont*.

(b)

```
Weight Sn particles and Si pieces
            │
            ▼
Synthesis the Ag-0.5Si master
       by arc-melting
            │
            ▼
Seal the Ag-0.5Si master in quartz tube
   and anneal at at 1000 ° C for 7 days
            │
            ▼
    Quench in cold water
            │
            ▼
  Weight Bi blocks, Ag particles
    and Al-0.5Si master alloy
            │
            ▼
   Seal in a vacuum quartz tube
    under an argon environment
            │
            ▼
Melt at 480 ° C for 12 h  ◄──  Homogenize by
                               melting three times
            │
            ▼
    Quench in cold water
```
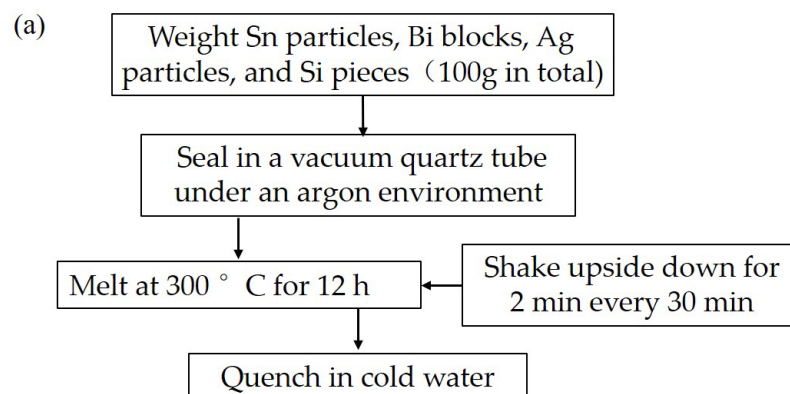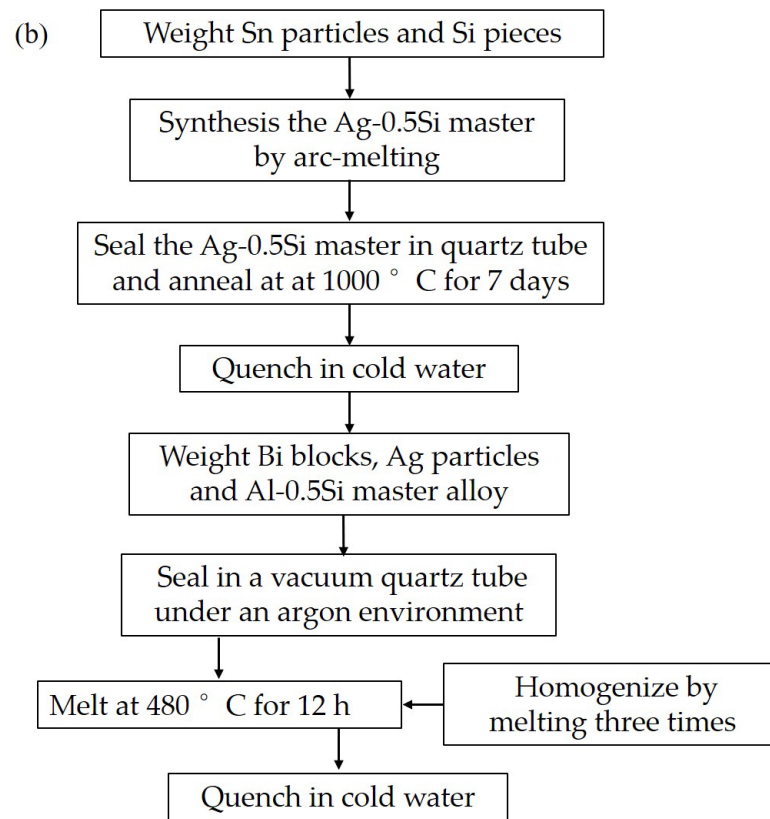
Figure 1. Schematic diagram of the samples' preparation: (**a**) Sn-Bi-Ag alloy and (**b**) Sn-Bi-Ag-Si alloy.

Prior to observing the alloy's microstructure, all samples were polished with 0.3 μm Al_2O_3 suspension. Scanning electron microscopy (JSM-6510, JEOL, Tokyo, Japan) combined with an energy-dispersive X-ray spectrometer (Oxford, UK) (SEM-EDS) was utilized to observe the microstructure. The probe diameter was 1 mm, and the acceleration voltage was 20 kV. The data in this work are the average of at least three measurements. Phase identification was performed by using a D/max 2500 PC X-ray diffractometer (Rigaku, Tokyo, Japan) and Cu Kα radiation for X-ray diffraction (XRD) measurements. Data in the 2θ range of 10–90° were collected, and the XRD patterns were indexed and calculated by the Jade 5.0 software.

A WDT-3030KN universal tensile tester was used to measure both the tensile strength and elongation of solders. A schematic diagram of the tensile test specimens in this work is shown in Figure 2. Tensile tests were performed with a loading speed of 1 mm/min at room temperature. The data in this work were the mean of at least five different measures. The microhardness of alloys was tested with a Vickers hardness tester (HXD-1000TMCLCD, XTZ, Shanghai, China) under a load of 0.245 N and a residence time of 5 s at room temperature.
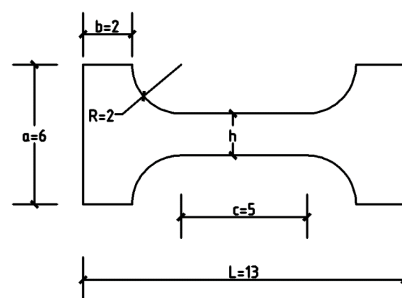
Figure 2. Schematic of tensile specimen dimensions.

To estimate the phase transition point of solder alloys, a NETZSCH DSC 404 F3 (METZSCH, Selb, Germany) differential scanning calorimeter was used at a heating rate of 10 °C/min. Wettability tests were carried out by using the hanging drop high-temperature wettability angle measuring instrument, during which drops of solder alloy liquid from a dropper fell onto a Cu plate on a platform. Interfacial reactions between the solder alloy and Cu plate were investigated by analyzing the cross-sectional microstructure of Cu sheets that were hot-dipped in a Sn-Bi-Ag-based alloy bath at 190 °C for 1 min.

3. Results and Discussion

3.1. Microstructure of Solder Alloys

Figure 3a shows an SEM image of the Sn-35Bi-1Ag solder alloy. Based on the differences in shape and brightness in the grayscale images, there were three different phases in the alloy. The composition of each typical region marked "P", "Q", and "N" in Figure 3a is shown in Figure 3b–d, respectively. Combined with the EDS analysis, the bright phase was (Bi), the grey matrix was (Sn), and there was a small amount of dark grey Ag_3Sn phase distributed throughout the (Sn) matrix. Most of the (Bi) phase existed as large granules, only a few of which were embedded in the (Sn) matrix. The characteristic peaks of the (Sn) and (Bi) phases were evident from the XRD patterns in Figure 4a,b. The Ag_3Sn phase was not observed, perhaps due to the small amount of Ag added.
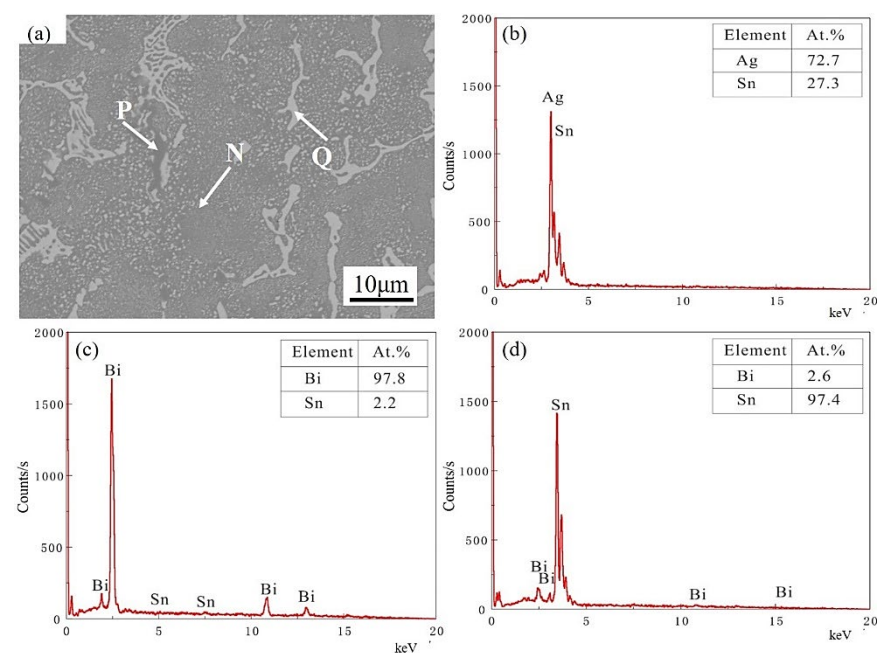
Figure 3. (**a**) SEM images of the Sn-35Bi-1Ag alloy, and (**b**–**d**) EDS profiles of regions marked "P", "Q", and "N", respectively.

Figure 5 shows the SEM images of the Sn-xBi-1Ag solder alloys with different Bi contents. More (Bi) precipitated as the Bi content increased. Figure 5 shows the SEM images of the Sn-xBi-1Ag-0.5Si solder alloys with different Bi contents. Similarly, the (Bi) phase grew as the Bi concentration rose. By comparing the SEM images in Figures 5 and 6, it can be seen that adding a small amount of Si refined the structure, and the (Bi) phase changed from large blocks to a smaller network. The amount of needle-like (Bi) phase embedded in the (Sn) matrix increased. A plausible explanation for this fine structure was that after adding particles, undercooling of the Sn-rich solder was reduced, thereby inhibiting the growth of intermetallic compounds and further refining the microstructure [39,40].
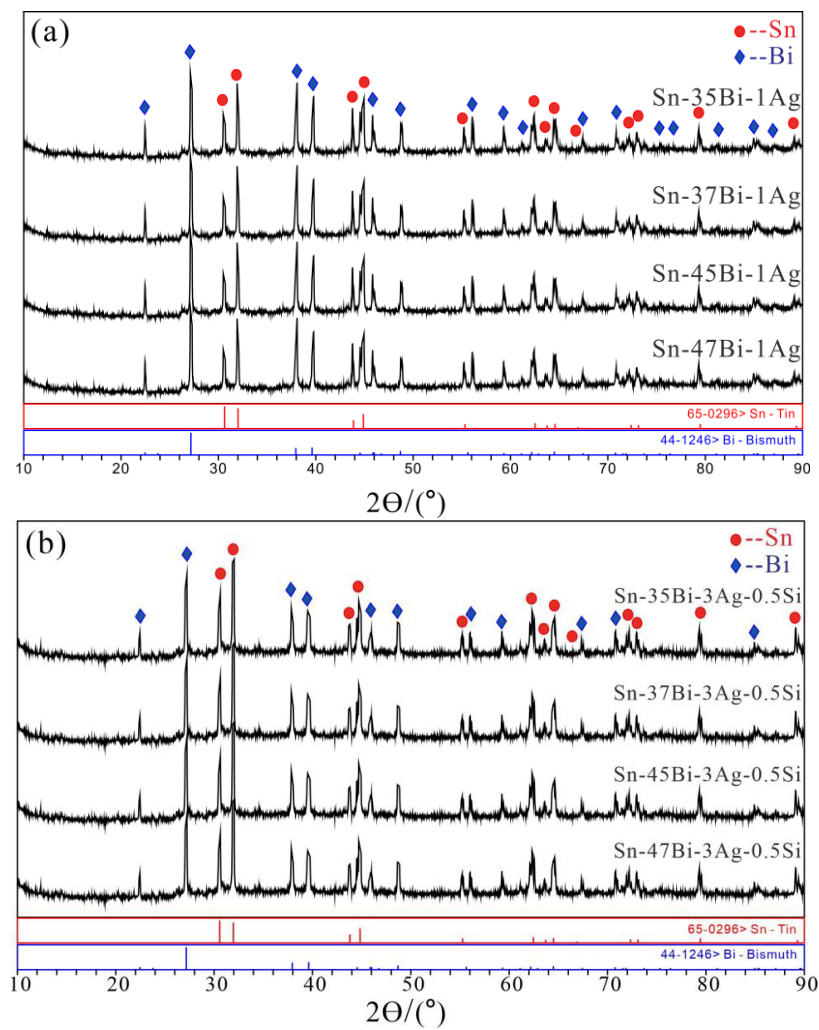
Figure 4. XRD patterns of (**a**) Sn-xBi-1Ag and (**b**) Sn-xBi-3Ag-0.5Si alloys.
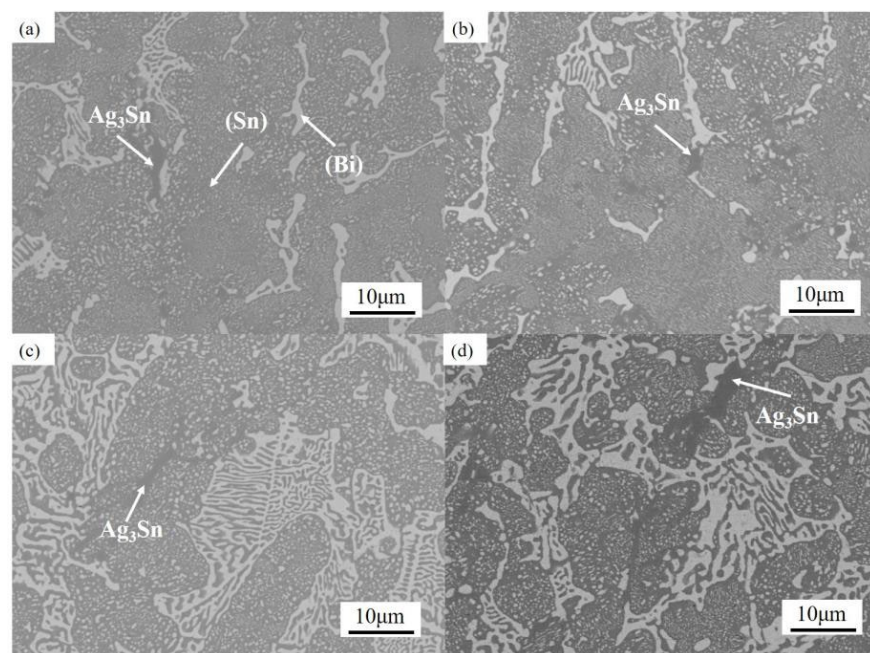
Figure 5. SEM images of the Sn-xBi-1Ag solder alloys: (**a**) $x = 35$, (**b**) $x = 37$, (**c**) $x = 45$, and (**d**) $x = 47$.
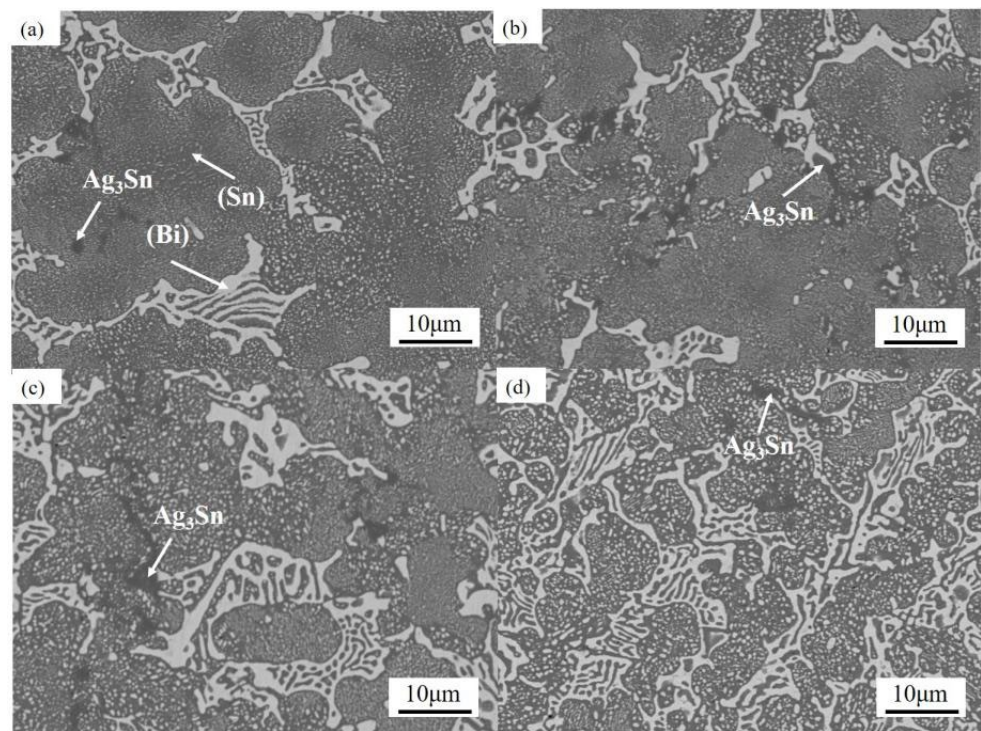
Figure 6. SEM images of the Sn-xBi-1Ag-0.5Si alloys: (**a**) *x* = 35, (**b**) *x* = 37, (**c**) *x* = 45, and (**d**) *x* = 47.

Figure 7 shows the SEM images of Sn-xBi-3Ag-0.5Si alloys with different Bi contents. Compared with Figure 5, the content of the dark black Ag_3Sn phase increased significantly upon increasing the Ag content. However, the Ag_3Sn phase was still not detected in the XRD patterns shown in Figure 4b as its content was still below the detection limit.
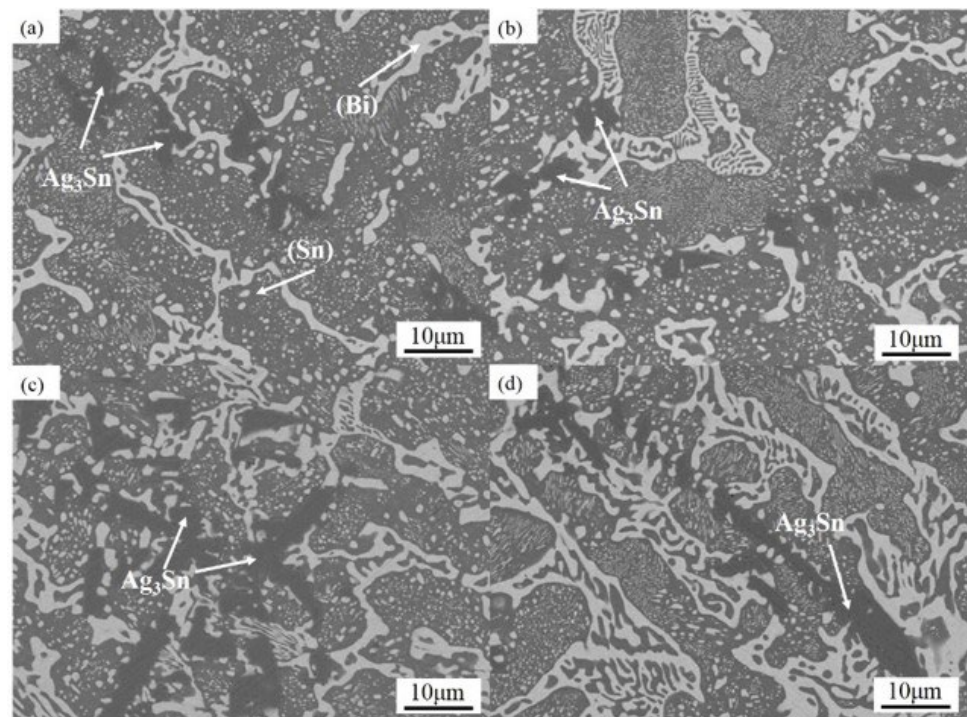
Figure 7. SEM images of the Sn-xBi-3Ag-0.5Si alloys: (**a**) *x* = 35, (**b**) *x* = 37, (**c**) *x* = 45, and (**d**) *x* = 47.

3.2. Mechanical Properties of the Solder Alloys

3.2.1. Tensile Strength

Solder alloys with a high tensile strength can help increase the solder's stability. Figure 8 shows the tensile strength of 12 kinds of solder alloys in this experiment. For Sn-xBi-1Ag solder alloys, when the Ag content remained unchanged, a higher Bi content decreased the tensile strength of the alloy. According to the microstructure shown in Figures 5–7, the (Bi) phase increased as the Bi concentration rose and segregation became more visible. The solid solution and precipitation of Bi in the Sn matrix improved the strength and hardness of the alloy, but this also reduced its plasticity and toughness. Therefore, the tensile strength of Sn-xBi-1Ag solder alloys declined as the Bi content increased.
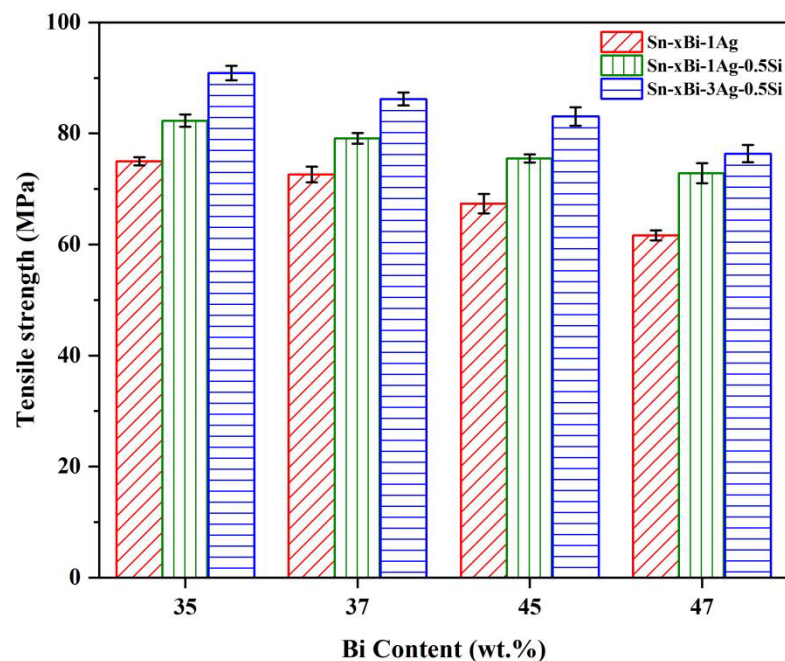
Figure 8. Tensile strength of solder alloys.

When the concentrations of Ag and Bi were identical, adding trace Si greatly increased the alloy's tensile strength, as shown in Figure 8. After adding a small amount of Si atoms to the Sn-45Bi-1Ag solder alloy, the tensile strength improved by 18.2%. The addition of trace Si might refine the eutectic phase, inhibiting the segregation of the coarse brittle (Bi) phase and reducing the alloy's brittleness. As a second-phase strengthening mechanism, the addition of Si enhanced the tensile strength of the solder alloy. When the Ag content of the Sn-xBi-yAg-0.5Si solder alloy increased, the alloy's tensile strength might have been further improved. The Sn-45Bi-3Ag-0.5Si alloy's tensile strength even exceeded that of the Sn-35Bi-1Ag-0.5Si alloy. The tensile strength of the Sn-35Bi-3Ag-0.5Si alloy reached 90.87 MPa. A plausible explanation is that as the Ag content increased, more Ag_3Sn phase precipitated in the alloy's microstructure. The Ag_3Sn phase in the solder alloy tended to be coarse, which prevented dislocation movement. Slip was hampered during deformation, resulting in unequal plastic deformation throughout the matrix. Finally, the local plastic constraint of the solder was strengthened, so that the solder alloy's tensile strength was greatly increased. When adding 2 wt.% Ag to the Sn-0.7Cu eutectic alloy, El-Daly and Hammad [41] also found that the Ag_3Sn phase formed in the microstructure enhanced the solder's tensile strength and elongation at break.

3.2.2. Microhardness

Figure 9 compares the microhardness of Sn-Bi-1Ag, Sn-Bi-1Ag-0.5Si, and Sn-Bi-3Ag-0.5Si series solder alloys. Compared with the microhardness of the Sn-Bi-1Ag alloy, these alloys showed a higher microhardness after adding 0.5 wt.% Si, an increase of about 4.5%.

The reason for this phenomenon was that Si inhibited the formation and segregation of coarse and brittle Bi in the alloy, which refined the microstructure. Figure 9 illustrates that the microhardness values of the Sn-Bi-3Ag-0.5Si solder alloys were all lower than those of the Sn-Bi-1Ag-0.5Si solder alloys. By comparing the microstructures shown in Figures 6 and 7, the excessive addition of Ag in the Sn-Bi-3Ag-0.5Si solder alloys led to a more coarse Ag_3Sn phase precipitating in the alloy, and the Bi content in the substrate was relatively higher than that in Sn-Bi-1Ag-0.5Si solder alloys, so more white tiny (Bi) were precipitated, resulting in a decrease in the microhardness of the alloys [42]. The size of the Ag_3Sn phase may also play a key role in limiting lamellae formation and microstructure refinement [29].
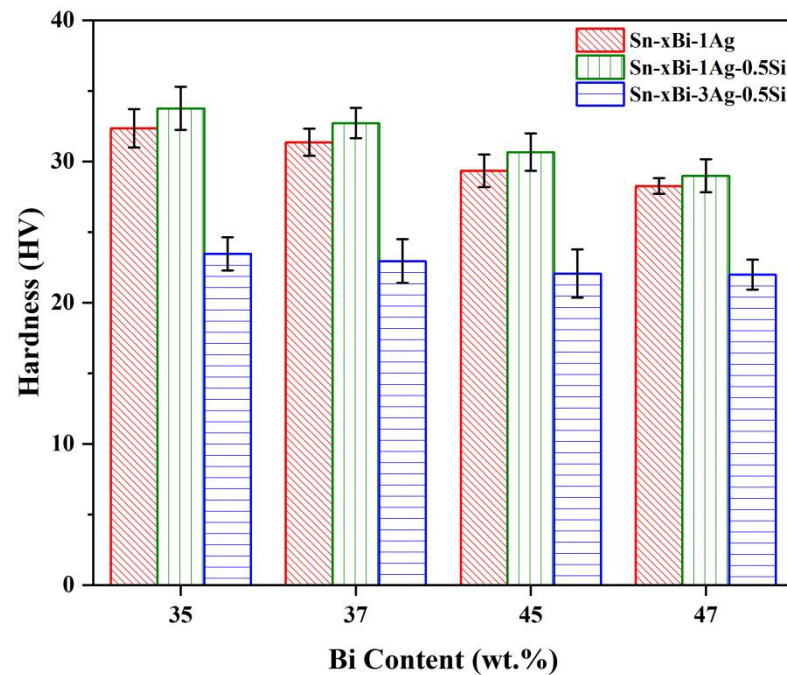
Figure 9. Microhardness of solder alloys.

For the Sn-Bi-1Ag series solders, the alloys' hardness and tensile strength both steadily declined as the Bi content increased. After adding a small amount of Si, the alloy's microhardness and tensile strength were both enhanced. The hardness of the Sn-Bi-Ag-0.5Si solder alloy decreased as the Ag percentage rose, while the tensile strength increased.

3.3. Melting Properties of the Solder Alloys

Figures 10–12 show the DSC curves of Sn-Bi-1Ag, Sn-Bi-1Ag-0.5Si, and Sn-Bi-3Ag-0.5Si series solder alloys. Here, the intersection of the tangent line at the maximum slope of the leading edge of the heat absorption peak in the DSC curve with the front baseline extension is T_m. In addition, the intersection of the tangent at the maximum slope of the trailing edge of the endothermic peak and the extension line of the back baseline is T_n. The difference between T_n and T_m is regarded as the melting range of the solder alloy. The values of T_m, T_n, and the melting ranges of the 12 solder alloys were collected in Tables 1–3.
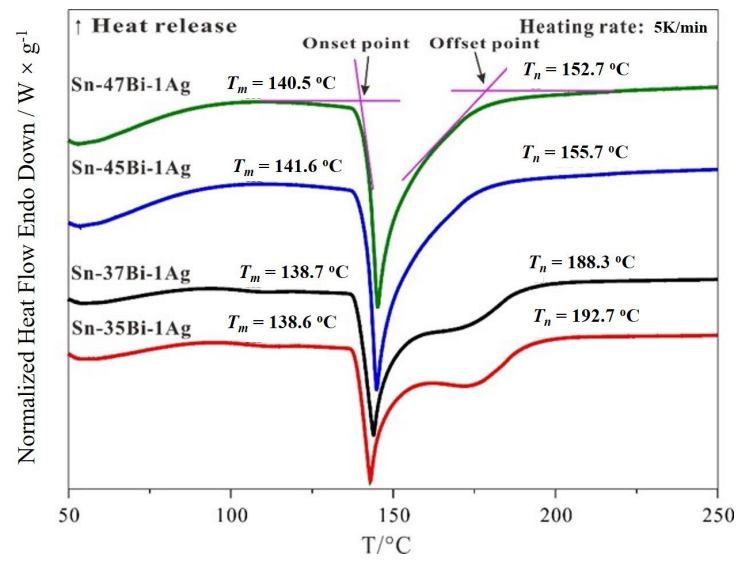
Figure 10. DSC curves of the Sn-xBi-Ag solder alloys.
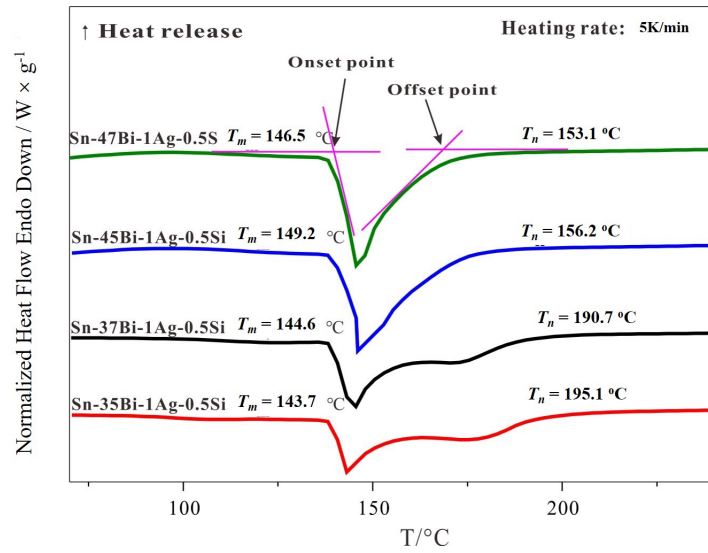
Figure 11. DSC curves of the Sn-xBi-1Ag-0.5Si solder alloys.
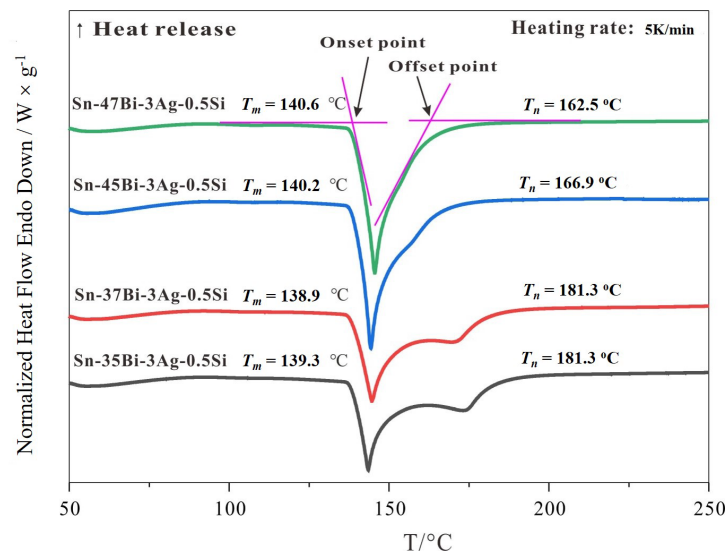
Figure 12. DSC curves of Sn-xBi-3Ag-0.5Si solder alloys.

Table 1. Phase transition temperature and melting range of the Sn-xBi-1Ag solder alloys.

Alloys	$T_m/°C$	$T_n/°C$	Melting Range/°C
Sn-35Bi-1Ag	138.6	192.7	54.1
Sn-37Bi-1Ag	138.7	188.3	49.6
Sn-45Bi-1Ag	141.6	155.7	14.1
Sn-47Bi-1Ag	140.5	152.7	12.2

Table 2. Phase transition temperature and melting range of the Sn-xBi-1Ag-0.5Si solder alloys.

Alloys	$T_m/°C$	$T_n/°C$	Melting Range/°C
Sn-35Bi-1Ag-0.5Si	139.5	195.1	55.6
Sn-37Bi-1Ag-0.5Si	139.6	190.7	51.1
Sn-45Bi-1Ag-0.5Si	142.2	156.2	14
Sn-47Bi-1Ag-0.5Si	141.3	153.1	11.8

Table 3. Phase transition temperature and melting range of the Sn-xBi-3Ag-0.5Si solder alloys.

Alloys	$T_m/°C$	$T_n/°C$	Melting Range/°C
Sn-35Bi-3Ag-0.5Si	139.3	183.3	44
Sn-37Bi-3Ag-0.5Si	138.9	181.3	42.4
Sn-45Bi-3Ag-0.5Si	140.2	166.9	26.7
Sn-47Bi-3Ag-0.5Si	140.6	162.5	21.9

Figure 10 shows that the DSC curves of the Sn-45Bi-1Ag and Sn-47Bi-1Ag solder alloys had only one main peak, while those of the Sn-35Bi-1Ag and Sn-37Bi-1Ag solder alloys also had a secondary peak near 165 °C. The secondary peak appeared because the alloy was incompletely melted after the eutectic reaction, and there were still primary phases that continued to melt. For the Sn-Bi-1Ag series solder alloys, as the Bi content increased from 35 wt.% to 47 wt.%, the starting temperature of the solder alloy did not change much. The difference was within 2 °C, and the main peak temperature was also basically the same. The termination point varied greatly, so changes in the Bi content affected the initial phase crystallization temperature of the alloy, i.e., the liquidus temperature. When there was only one main peak in the curve, the melting range was within 15 °C. When a secondary peak appeared, the melting range of the alloy broadened significantly to 50 °C. The melting range of the alloy steadily widened as the Bi concentration decreased and the secondary peak value increased. The termination point temperature gradually decreased as the Bi concentration rose, i.e., the temperature required to completely melt the solder alloy decreased continuously. Billah et al. [43] suggested that the temperature required for complete melting gradually decreased as the Bi content increased and approached the eutectic point of the Sn-Bi binary alloy.

The DSC curves of Sn-Bi-Ag-0.5Si solder alloys with different Bi contents are shown in Figure 11. Comparing Figures 10 and 11, as well as Tables 1 and 2, shows that the starting melting temperature of the solder alloy remained almost unchanged after adding 0.5 wt.% Si to the Sn-Bi-Ag series solder alloys, which have a maximum difference of only 0.9 °C. The main peak temperature and the secondary peak temperature were basically the same. In addition, the termination point did not significantly change, showing that the Bi content had no discernible influence on the solder alloy's melting range.

Figure 12 shows the DSC curves of the Sn-xBi-3Ag-0.5Si series solder alloys with different Ag contents. Table 3 shows the starting melting temperature of the Sn-xBi-3Ag-0.5Si solder alloy. Increasing the Ag content in the Sn-Bi-Ag-0.5Si series solder alloys produced essentially no change in the onset point of the Sn-Bi-Ag-Si solder alloy and had no significant effect on the primary and secondary peak temperatures. Nevertheless, when the Bi content was low (≤37 wt.%), the termination temperature of the alloys diminished marginally, and the maximum difference reached 11.8 °C. When the Bi content exceeded

45 wt.%, the termination temperature of the solder alloy increased, and the maximum difference reached 10.7 °C. When the Bi content was less than 40 wt.%, the inclusion of Ag limited the alloy's melting range due to interactions between Ag and Sn, which produced the intermetallic complex Ag_3Sn. The melting point of the eutectic compound was lower than that of Sn, and Sn was consumed during the generation of the compound. As more Ag was added, more Sn was consumed, which resulted in little change in the liquid phase line temperature and a decrease in the solid phase line temperature. This led to a reduction in the solder alloy's melting range. When the Bi content was too high ($\geq$45 wt.%), as more Ag was added, the solidus temperature increased while the liquidus temperature did not change much, thus increasing the alloy's melting range.

3.4. Wettability of the Solder Alloys

Wettability is a crucial metric for determining the solderability of an alloy. Generally, wettability is reflected by the contact angle of the solder alloy on a Cu substrate, which may be affected by many factors, such as surface roughness and operating parameters [44]. To evaluate the wettability of solder alloys, we measured the contact angle of molten solder alloy droplets on a Cu plate. In general, a smaller contact angle indicates better wettability of the solder alloy toward the Cu sheet.

Figures 13–15 show the wetting spreading diagrams of Sn-xBi-1Ag, Sn-xBi-1Ag-0.5Si, and Sn-xBi-1Ag-0.5Si solders on a Cu sheet, respectively. The contact angle curves of all solder alloys are shown in Figure 16. The contact angle of Sn-Bi-Ag series solder alloys on Cu substrates decreased upon increasing the Bi content. Bismuth improved the alloy's wettability because it is a surface-active element that can depress the interfacial tension of welding materials. Although the wettability of the alloys was better, the contact angle remained high. Furthermore, the contact angle of the Sn-35Bi-1Ag-0.5Si solder alloy on the Cu sheet was 65°, which was approximately 35% lower than that of the Sn-35Bi-1Ag solder alloy. When the Bi content reached 45 wt.%, the contact angle was approximately 33.5°.
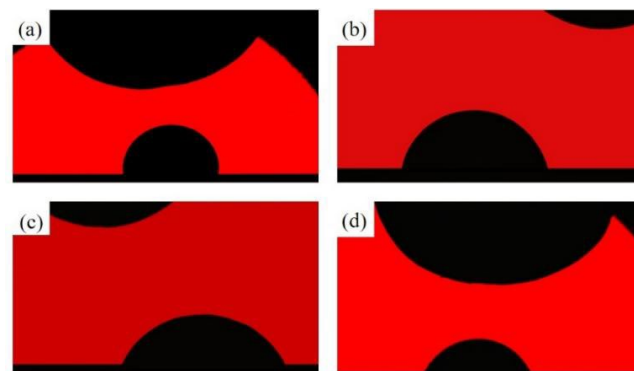
Figure 13. The spreading diagram of Sn-xBi-1Ag solder alloys dropped on a Cu substrate: (**a**) *x* = 35, (**b**) *x* = 37, (**c**) *x* = 45, and (**d**) *x* = 47.
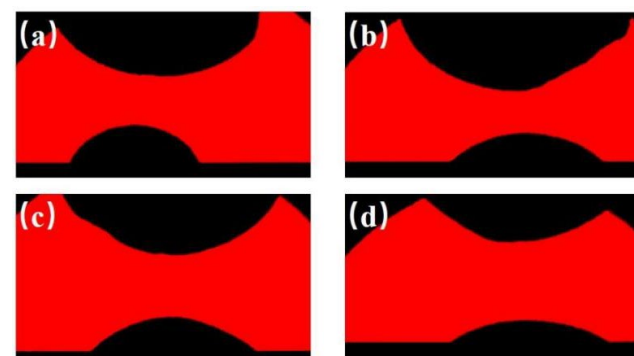
Figure 14. The spreading diagram of Sn-xBi-1Ag-0.5Si solder alloys dropped on a Cu substrate: (**a**) *x* = 35, (**b**) *x* = 37, (**c**) *x* = 45, and (**d**) *x* = 47.
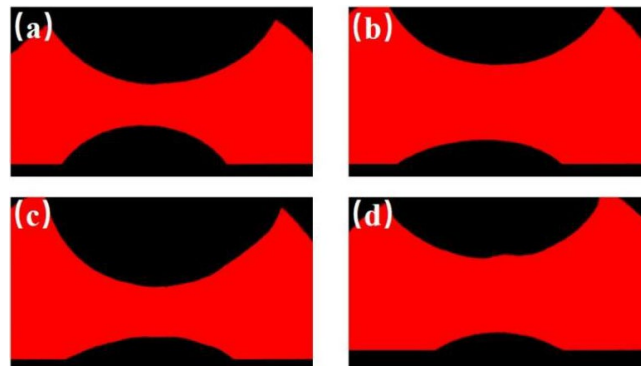
Figure 15. The spreading diagram of Sn-xBi-3Ag-0.5Si solder alloys dropped on a Cu substrate: (**a**) *x* = 35, (**b**) *x* = 37, (**c**) *x* = 45, and (**d**) *x* = 47.
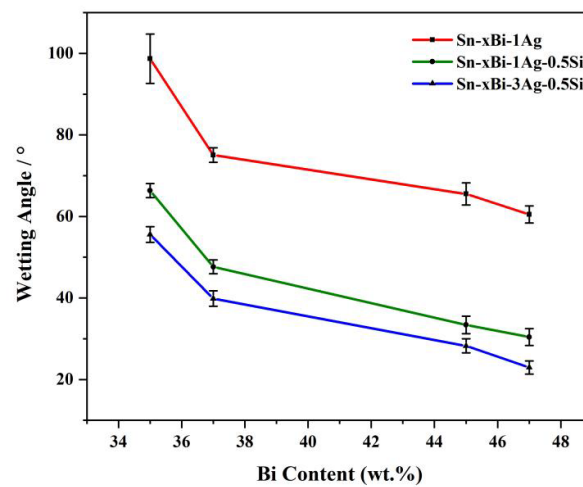
Figure 16. Comparison of the wetting angles of the Sn-xBi-1Ag, Sn-xBi-1Ag-0.5Si, and Sn-xBi-3Ag-0.5Si solder solutions on a Cu substrate.

When the contact angle was greater than 0 and less than 20°, the wettability was excellent, but when the contact angle was higher than 40°, the wettability was poor [45]. As shown in Figure 16, the contact angles of Sn-Bi-3Ag-0.5Si series solders on Cu sheets were usually small, and the contact angle of Sn-47Bi-3Ag-0.5Si solder was even close to 20°. Since the surface tension of Ag is very low (0.03 N/m), the addition of Ag reduced the surface tension of the Sn-Bi-Ag-Si series solder alloys, thereby reducing their contact angle on the Cu sheet and increasing their wettability, which was consistent with the results of this experiment. In addition, due to the wetting and diffusion of molten solder on the Cu substrate, an intermetallic compound layer formed at the interface. This thin intermetallic compound layer helped ensure a strong metal bonding between the molten solder and Cu. However, an excessively thick compound layer increased the surface tension. Silver atoms reduced the surface tension of Sn on the compound layer, thereby reducing the surface tension of the solder on the Cu substrate. Therefore, upon increasing the Ag content, the wettability of the Sn-Bi-Ag-Si solder alloy was improved. In summary, the wettability of the Sn-45Bi-1Ag-0.5Si, Sn-47Bi-1Ag-0.5Si, Sn-45Bi-3Ag-0.5Si, and Sn-47Bi-3Ag-0.5Si solders were all superior to that of the traditional $Sn_{60}Pb_{40}$ solder.

3.5. Interfacial Reactions of the Solder Alloys with Cu Sheet

The formation of a thin and continuous intermetallic compound layer during welding is necessary for good wetting and connections and improves the mechanical properties of solder joints [46]. However, since intermetallic compounds are brittle, an excessively thick compound layer will significantly reduce the reliability of solder joints.

Figure 17 shows the SEM images of the interface between the Sn-xBi-1Ag solder and Cu substrate after reacting at 190 °C for 1 min. The EDS analysis showed that the IMC layer was Cu_6Sn_5 phase. In addition, (Sn), (Bi), and Ag_3Sn phases were observed close to the Cu_6Sn_5 IMC layer. This indicated that Sn in the solder solution preferentially diffused throughout the Cu matrix, while Bi and Ag atoms did not react with the Cu matrix. The formation and growth of the Cu_6Sn_5 layer were mainly controlled by diffusion. Cu atoms were dissolved in a molten Sn-based solder and reacted with Sn atoms. The relationship between the thickness of the Cu_6Sn_5 IMC layer and the Bi content is shown in Figure 18. A higher Bi content decreased the thickness of the IMC layer, probably because of the content of Sn atoms in the solder. As shown in Figure 16, the wetting angles of the Sn-xBi-Ag solder solutions on the Cu substrate decreased with increasing Bi content, which facilitated the interfacial reaction between Cu and Sn. When the Cu substrate was covered with Cu-Sn IMC, the interfacial reaction would be inhibited and the thickness of Cu-Sn IMC would be limited. So, a higher Bi content restricted the development of the IMC layer.
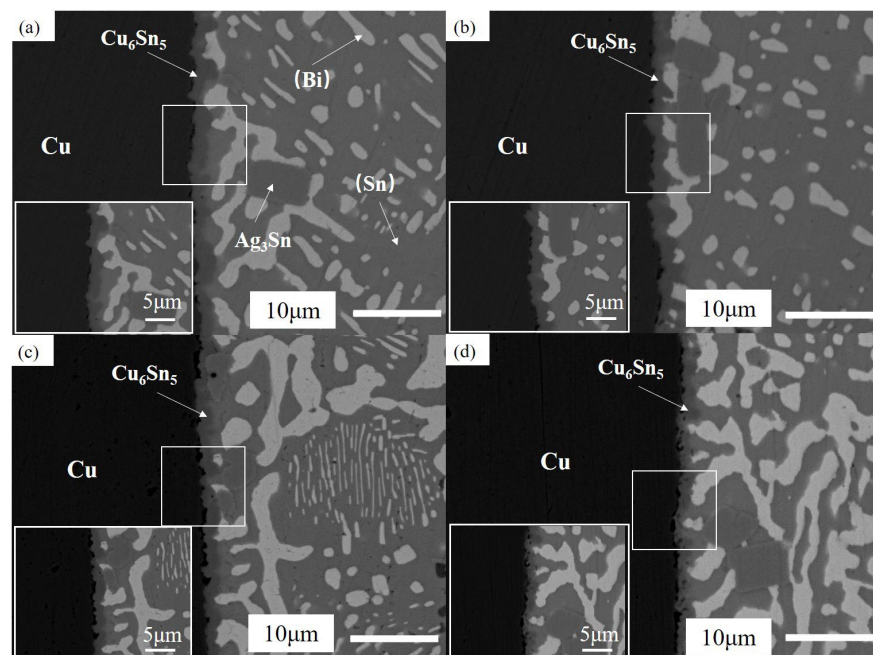
Figure 17. SEM images showing the interfacial morphology of Sn-xBi-1Ag/Cu at 190 °C: (**a**) x = 35, (**b**) x = 37, (**c**) x = 45, and (**d**) x = 47.
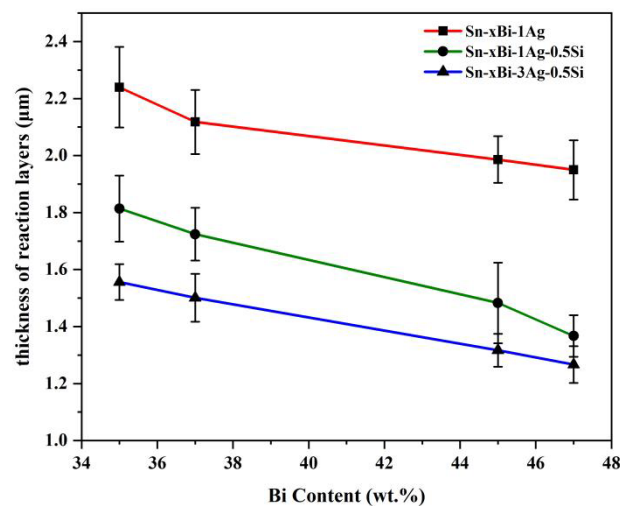
Figure 18. Thickness of solder/Cu reaction layers.

Figure 19 shows the SEM images of the interface between the Sn-xBi-1Ag-0.5Si solder and Cu substrate after reacting at 190 °C for 1 min. The IMC's thickness decreased due to the addition of Si. In particular, when the Bi content was 45 wt.%, the thickness of the interfacial reaction layer decreased by nearly 42% after adding Si. The addition of Si did not result in the formation of intermetallic compounds but only formed Si particles, which hindered the diffusion of Cu atoms into the molten solder. Figure 20 shows the SEM images of the interface between the Sn-xBi-3Ag-0.5Si alloy and Cu substrate after reacting at 190 °C for 1 min. The IMC layer's thicknesses of Sn-35Bi-3Ag-0.5Si/Cu and Sn-37Bi-3Ag-0.5Si/Cu were much thinner than those of Sn-35Bi-1Ag-0.5Si/Cu and Sn-37Bi-1Ag-0.5Si/Cu. Upon increasing the Ag content, the Ag_3Sn phase content greatly increased and coarsened, which hindered interfacial passage during atomic diffusion and reduced the interface growth rate. Therefore, the formation and growth of an IMC layer at the interface were inhibited. The Ag_3Sn phase helped improve the strength of the matrix at the front of the IMC layer, which helped inhibit the fracture of Sn-Bi-Ag-Si/Cu joints in the matrix and made them more likely to occur at the intersection between the matrix and IMC layer.
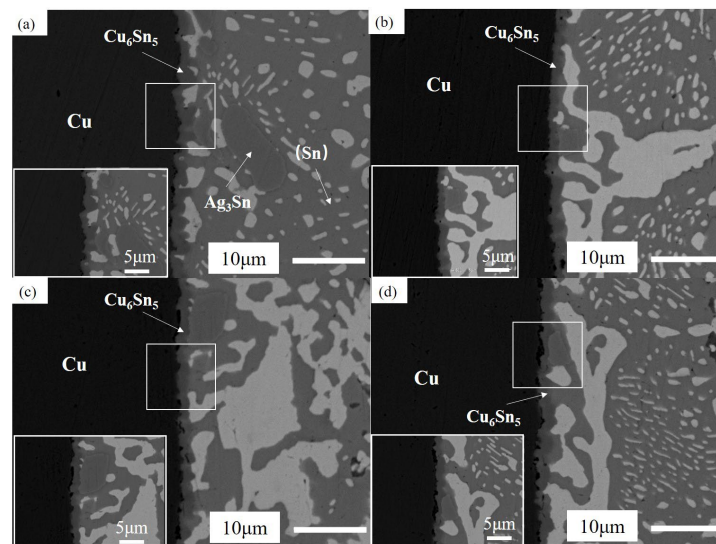
Figure 19. SEM images showing the interfacial morphology of Sn-xBi-1Ag-0.5Si/Cu at 190 °C: (**a**) $x = 35$, (**b**) $x = 37$, (**c**) $x = 45$, and (**d**) $x = 47$.
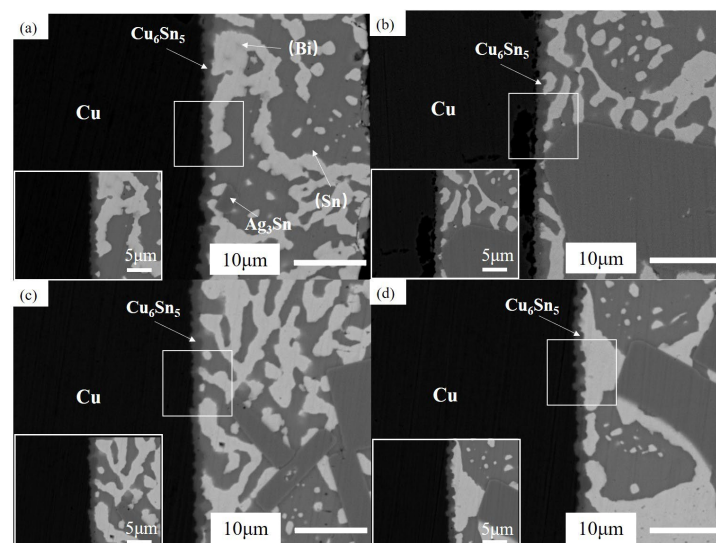
Figure 20. SEM images showing the interfacial morphology of Sn-xBi-3Ag-0.5Si/Cu at 190 °C: (**a**) $x = 35$, (**b**) $x = 37$, (**c**) $x = 45$, and (**d**) $x = 47$.

4. Conclusions

The main conclusions of this experiment were as follows:

(1) For Sn-x ($x = 35, 37, 45$, and 47) Bi-1Ag solder alloys, the segregation of Bi became more obvious, and bright, irregular-shaped areas continued to increase upon increasing the Bi content. The mechanical properties of the alloy decreased upon increasing the Bi content, and the melting point and melting range were slightly reduced, but the wettability was improved. The thickness of the Cu_6Sn_5 IMC layer decreased upon increasing the Bi content.

(2) After adding Si to the Sn-xBi-1Ag alloy, the structure was refined. In particular, the size of the Bi phase decreased from the large blocks into a network shape. The amount of needle-like Bi phase embedded in the Sn matrix increased. After adding trace Si, the melting point and melting range of the alloys did not markedly change, while tensile strength and hardness were improved, the wettability was optimized, and the thickness of the diffusion layer formed with the Cu substrate was significantly reduced.

(3) Upon increasing the Ag content in the Sn-Bi-Ag-0.5Si alloy, the dark black Ag_3Sn phase increased significantly. The tensile strength of the Sn-Bi-Ag-0.5Si solder continued to increase, while its hardness decreased slightly. The melting point and melting range increased slightly. Moreover, the wettability of the Sn-Bi-3Ag-0.5Si series solder alloys improved greatly, and the width of the Cu_6Sn_5 layer decreased.

Author Contributions: Conceptualization, Y.L. (Ya Liu) and Z.G.; methodology, S.C., X.W. and X.S.; validation, S.C., X.W. and C.W.; formal analysis, S.C. and X.W.; investigation, S.C., X.W. and Y.L. (Yongxiong Liu); resources, S.C. and X.W.; data curation, S.C. and X.W.; writing—original draft preparation, S.C. and X.W.; writing—review and editing, Y.L. (Ya Liu); visualization, S.C. and X.W.; supervision, Z.G. and Y.L. (Ya Liu). All authors have read and agreed to the published version of the manuscript.

Institutional Review Board Statement: Not applicable.

Informed Consent Statement: Not applicable.

Data Availability Statement: Not applicable.

Conflicts of Interest: The authors declare no conflict of interest.

References

1. Garcia, L.R.; Osório, W.R.; Peixoto, L.C.; Garcia, A. Wetting Behavior and Mechanical Properties of Sn-Zn and Sn-Pb Solder Alloys. *J. Electron. Mater.* **2009**, *38*, 2405–2414. [CrossRef]
2. Qiu, H.; Hu, X.; Li, S.; Wan, Y.; Li, Q. Shear strength and fracture surface analysis of lead-free solder joints with high fraction of IMCs. *Vacuum* **2020**, *180*, 109611. [CrossRef]
3. Chen, G.; Liu, L.; Silberschmidt, V.V.; Liu, C.; Wu, F.; Chan, Y.C. Microstructural evolution of 96.5Sn–3Ag–0.5Cu lead free solder reinforced with nickel-coated graphene reinforcements under large temperature gradient. *J. Mater. Sci. Mater. Electron.* **2018**, *29*, 5253–5263. [CrossRef]
4. Dias, M.; Costa, T.A.; Soares, T.; Silva, B.L.; Cheung, N.; Spinelli, J.E.; Garcia, A. Tailoring Morphology and Size of Microstructure and Tensile Properties of Sn-5.5 wt.%Sb-1 wt.%(Cu,Ag) Solder Alloys. *J. Electron. Mater.* **2018**, *47*, 1647–1657. [CrossRef]
5. Mahmudi, R.; Mahin-Shirazi, S. Effect of Sb addition on the tensile deformation behavior of lead-free Sn–3.5Ag solder alloy. *Mater. Des.* **2011**, *32*, 5027–5032. [CrossRef]
6. George, E.; Pecht, M. RoHS compliance in safety and reliability critical electronics. *Microelectron. Reliab.* **2016**, *65*, 1–7. [CrossRef]
7. Yuan, Y.; Chen, X.; Zhou, Z.; Li, Y.; Xu, B.; Liu, D.; Yang, B. Theoretical study on Sn–Sb-based lead-free solder by ab initio molecular dynamics simulation. *J. Mater. Res.* **2019**, *34*, 2543–2553. [CrossRef]
8. Ren, G.; Collins, M.N. The effects of antimony additions on microstructures, thermal and mechanical properties of Sn-8Zn-3Bi alloys. *Mater. Des.* **2017**, *119*, 133–140. [CrossRef]
9. Han, Y.; Gao, Y.; Jing, H.; Wei, J.; Zhao, L.; Xu, L. A modified constitutive model of Ag nanoparticle-modified graphene/Sn–Ag–Cu/Cu solder joints. *Mater. Sci. Eng. A* **2020**, *777*, 139080. [CrossRef]

10. Shen, Y.-A.; Chen, S.-W.; Chen, H.-Z.; Chang, C.-M.; Ouyang, Y.-H. Extremely thin interlayer of multi-element intermetallic compound between Sn-based solders and FeCoNiMn high-entropy alloy. *Appl. Surf. Sci.* **2021**, *558*, 149945. [CrossRef]

11. Wei, Y.; Liu, Y.; Zhao, X.; Tan, C.; Dong, Y.; Zhang, J. Effects of minor alloying with Ge and In on the interfacial microstructure between Zn–Sn solder alloy and Cu substrate. *J. Alloys Compd.* **2020**, *831*, 154812. [CrossRef]

12. Zhou, S.; Yang, C.-H.; Shen, Y.-A.; Lin, S.-K.; Nishikawa, H. The newly developed Sn–Bi–Zn alloy with a low melting point, improved ductility, and high ultimate tensile strength. *Materialia* **2019**, *6*, 100300. [CrossRef]

13. Wang, Y.; Zhao, X.-C.; Liu, Y.; Wang, Y.; Li, D.-M. Microstructure, wetting property of Sn–Ag–Cu–Bi–xCe solder and IMC growth at solder/Cu interface during thermal cycling. *Rare Met.* **2021**, *40*, 714–719. [CrossRef]

14. Durga, A.; Wollants, P.; Moelans, N. Phase-field study of IMC growth in Sn–Cu/Cu solder joints including elastoplastic effects. *Acta Mater.* **2020**, *188*, 241–258. [CrossRef]

15. Yang, J.; Zhang, Q.; Song, Z. Influences of Ag and In Alloying on Microstructure and Mechanical Properties of Sn-58Bi Solder. *J. Electron. Mater.* **2021**, *50*, 283–290. [CrossRef]

16. Shen, Y.-A.; Chen, H.-Z.; Chen, S.-W.; Chiu, S.-K.; Guo, X.-Y.; Hsieh, Y.-P. Graphene as a diffusion barrier at the interface of Liquid–State low-melting Sn–58Bi alloy and copper foil. *Appl. Surf. Sci.* **2022**, *578*, 152108. [CrossRef]

17. Miao, H.-W.; Duh, J.-G. Microstructure evolution in Sn–Bi and Sn–Bi–Cu solder joints under thermal aging. *Mater. Chem. Phys.* **2001**, *71*, 255–271. [CrossRef]

18. Hirata, Y.; Yang, C.-H.; Lin, S.-K.; Nishikawa, H. Improvements in mechanical properties of Sn–Bi alloys with addition of Zn and In. *Mater. Sci. Eng. A* **2021**, *813*, 141131. [CrossRef]

19. Wu, X.; Wu, J.; Wang, X.; Yang, J.; Xia, M.; Liu, B. Effect of In addition on microstructure and mechanical properties of Sn–40Bi alloys. *J. Mater. Sci.* **2020**, *55*, 3092–3106. [CrossRef]

20. Chen, X.; Xue, F.; Zhou, J.; Yao, Y. Effect of In on microstructure, thermodynamic characteristic and mechanical properties of Sn–Bi based lead-free solder. *J. Alloys Compd.* **2015**, *633*, 377–383. [CrossRef]

21. Li, C.; Yan, Y.; Gao, T.; Xu, G. The influence of Ag on the microstructure, thermal properties and mechanical behavior of Sn–25Sb-xAg high temperature lead-free solder. *Vacuum* **2021**, *185*, 110015. [CrossRef]

22. Jiang, N.; Zhang, L.; Gao, L.-L.; Song, X.-G.; He, P. Recent advances on SnBi low-temperature solder for electronic interconnections. *J. Mater. Sci. Mater. Electron.* **2021**, *32*, 22731–22759. [CrossRef]

23. Xu, K.-K.; Zhang, L.; Gao, L.-L.; Jiang, N.; Zhang, L.; Zhong, S.-J. Review of microstructure and properties of low temperature lead-free solder in electronic packaging. *Sci. Technol. Adv. Mater.* **2020**, *21*, 689–711. [CrossRef]

24. Hu, F.; Zhang, Q.; Jiang, J.; Song, Z. Influences of Ag addition to Sn-58Bi solder on SnBi/Cu interfacial reaction. *Mater. Lett.* **2018**, *214*, 142–145. [CrossRef]

25. Mei, Z.; Morris, J.W. Characterization of eutectic Sn-Bi solder joints. *J. Electron. Mater.* **1992**, *21*, 599–607. [CrossRef]

26. Myung, W.-R.; Ko, M.-K.; Kim, Y.; Jung, S.-B. Effects of Ag content on the reliability of LED package component with Sn–Bi–Ag solder. *J. Mater. Sci. Mater. Electron.* **2015**, *26*, 8707–8713. [CrossRef]

27. Silva, B.L.; Garcia, A.; Spinelli, J.E. Complex eutectic growth and Bi precipitation in ternary Sn-Bi-Cu and Sn-Bi-Ag alloys. *J. Alloys Compd.* **2017**, *691*, 600–605. [CrossRef]

28. Gain, A.K.; Zhang, L. Effect of Ag nanoparticles on microstructure, damping property and hardness of low melting point eutectic tin–bismuth solder. *J. Mater. Sci. Mater. Electron.* **2017**, *28*, 15718–15730. [CrossRef]

29. Yang, T.; Zhao, X.; Xiong, Z.; Tan, W.; Wei, Y.; Tan, C.; Yu, X.; Wang, Y. Improvement of microstructure and tensile properties of Sn–Bi–Ag alloy by heterogeneous nucleation of β-Sn on Ag3Sn. *Mater. Sci. Eng. A* **2020**, *785*, 139372. [CrossRef]

30. Li, Y.; Chan, Y. Effect of silver (Ag) nanoparticle size on the microstructure and mechanical properties of Sn58Bi–Ag composite solders. *J. Alloys Compd.* **2015**, *645*, 566–576. [CrossRef]

31. Dong, W.; Shi, Y.; Xia, Z.; Lei, Y.; Guo, F. Effects of Trace Amounts of Rare Earth Additions on Microstructure and Properties of Sn-Bi-Based Solder Alloy. *J. Electron. Mater.* **2008**, *37*, 982–991. [CrossRef]

32. Wang, Z.; Zhang, Q.K.; Chen, Y.X.; Song, Z.L. Influences of Ag and In alloying on Sn-Bi eutectic solder and SnBi/Cu solder joints. *J. Mater. Sci. Mater. Electron.* **2019**, *30*, 18524–18538. [CrossRef]

33. Qin, W.; Li, J.; Zhang, Q.; Jiang, S.; Feng, J.; Yang, W.; Zhan, Y. Effect of addition of Al and Cu on the properties of Sn–20Bi solder alloy. *J. Mater. Sci. Mater. Electron.* **2022**, *33*, 177–189. [CrossRef]

34. Guo, Q.; Zhao, Z.; Shen, C. Comparison study on microstructure and mechanical properties of Sn-10Bi and Sn-Ag-Cu solder alloys and joints. *Microelectron. Reliab.* **2017**, *78*, 72–79. [CrossRef]

35. Ye, D.; Du, C.; Wu, M.; Lai, Z. Microstructure and mechanical properties of Sn–xBi solder alloy. *J. Mater. Sci. Mater. Electron.* **2015**, *26*, 3629–3637. [CrossRef]

36. Lai, Z.; Ye, D. Microstructure and fracture behavior of non eutectic Sn–Bi solder alloys. *J. Mater. Sci. Mater. Electron.* **2016**, *27*, 3182–3192. [CrossRef]

37. Karim, M.R.A.; Daniel, S.; Ul Haq, E.; Ahmad, A.; Khan, K.I.; Raza, S.A. Raza. Improving the Corrosion Resistance of API X56 and API X70 Pipeline Steels by Hot Dip Aluminization. In *Key Engineering Materials*; Trans Tech Publications Ltd.: Bäch, Switzerland, 2021; Volume 875, p. 315. [CrossRef]

38. Kab, M.; Mendil, S.; Taibi, K. Evolution of the Microstructure of Intermetallic Compounds Formed on Mild Steel During Hot Dipping in Molten Aluminum Alloy Baths. *Met. Microstruct. Anal.* **2020**, *9*, 476–483. [CrossRef]

39. Silva, B.L.; Garcia, A.; Spinelli, J.E. Cooling thermal parameters and microstructure features of directionally solidified ternary Sn–Bi–(Cu,Ag) solder alloys. *Mater. Charact.* **2016**, *114*, 30–42. [CrossRef]

40. Dias, M.; Costa, T.; Rocha, O.; Spinelli, J.E.; Cheung, N.; Garcia, A. Interconnection of thermal parameters, microstructure and mechanical properties in directionally solidified Sn–Sb lead-free solder alloys. *Mater. Charact.* **2015**, *106*, 52–61. [CrossRef]

41. El-Daly, A.; Hammad, A. Development of high strength Sn–0.7Cu solders with the addition of small amount of Ag and In. *J. Alloys Compd.* **2011**, *509*, 8554–8560. [CrossRef]

42. Kim, K.; Huh, S.; Suganuma, K. Effects of cooling speed on microstructure and tensile properties of Sn–Ag–Cu alloys. *Mater. Sci. Eng. A* **2002**, *333*, 106–114. [CrossRef]

43. Billah, M.; Shorowordi, K.M.; Sharif, A. Effect of micron size Ni particle addition in Sn–8Zn–3Bi lead-free solder alloy on the microstructure, thermal and mechanical properties. *J. Alloys Compd.* **2014**, *585*, 32–39. [CrossRef]

44. Gain, A.K.; Zhang, L. Interfacial microstructure, wettability and material properties of nickel (Ni) nanoparticle doped tin–bismuth–silver (Sn–Bi–Ag) solder on copper (Cu) substrate. *J. Mater. Sci. Mater. Electron.* **2015**, *26*, 3982–3994. [CrossRef]

45. Kripesh, V.; Teo, P.-S.; Tai, C.; Vishwanadam, G.; Mui, Y.C. Development of a Lead Free Chip Scale Package for Wireless Applications. In *51st Electronic Components and Technology Conference Proceedings*; IEEE: Piscataway, NJ, USA, 2001. [CrossRef]

46. Cheng, J.; Hu, X.; Jiang, X. Interfacial reaction and IMC growth between Sn-37 Pb and heterogeneous dual-phase substrate. *Vacuum* **2019**, *159*, 112–124. [CrossRef]